Dynamics of particle-laden thin films: viscous fluid on an incline

Sarah Burnett[1], Jesse Kreger[2], Hanna Kristensen[3], and Andrew Stocker[4]

[1] *University of North Carolina, Chapel Hill*
[2] *Occidental College*
[3] *Pepperdine University*
[4] *University of San Francisco*

August 7, 2015

Abstract

We present experimental results of the height profile of particle-laden viscous thin films with finite volume on an incline. For high angles of inclination and high concentrations of mixtures, negatively buoyant particles undergo resuspension then accumulate at the front of the suspending fluid; this leads to the development of a particle-rich 'ridge'. Theoretically, the ridge corresponds to the shocks which take on two characteristic shapes: singular and double shocks. We observe the presence of both formations experimentally by varying the volume of the slurry and compare our results to the theoretical model. Our research also investigates the dependence of the fingering instability as the inclination angle or particle to liquid concentration is changed. The slurries have similar dynamics to those used in coating flow techniques and other industrial applications.

Contents

1 Introduction

Thin film viscous particle slurries occur frequently in applications ranging from spiral separators in the mining industry to Bostwick consistometers in the food industry [5]. Despite their ubiquity, the dynamics of the slurry, particularly that of the front, are not fully understood. Previous work has focused on modeling the movement of the slurry down an incline for various concentrations and inclination angles with a free surface and contact lines. This has given rise to a mathematical model that predicts the formation of a characteristic shock depending on initial conditions. Experimentally, the model is tested by monitoring the movement of the front down the incline and comparing results to a numerical solution.

The particle-laden fluid is an approximately uniform mixture of solid spheres of similar diameter in a viscous oil. For rigid spherical single particles in viscous fluid, Stokes Law applies. A hindrance equation modifies the velocity given by Stokes law to account for collisions impeding settling for large particle volume fractions, ϕ. The particles are negatively buoyant, and thus in the absence of outside forces they tend to settle due to gravity. As the fluid flows down the incline it is subject to shear stresses; this acts as a diffusive mechanism resulting from gradients in the particle volume fraction and suspension viscosity, $\mu(\phi)$. Shear stresses cause shear-induced migration, in which particles migrate towards areas of lower collision frequency and shear. The particles go through settling and resuspension as the fluid flows down the incline, keeping the mixture from separating [4].

The large-scale dynamics of the fluid front are determined by a difference in particle and liquid volumetric fluxes. Resuspension happens to varying degrees depending on the particle concentration and inclination angle, α, impacting these fluxes. It has been well documented that particle-laden thin film experiments can be partitioned by three different regimes: settled, well-mixed, and ridged [3]. For small concentrations and inclination angles, resuspension is minimized. This causes stratification of the suspension, where the clear fluid overtakes the particles and flows over them. This is referred to as the settled regime. For intermediate particle concentrations and inclination angles the difference in fluxes is approximately zero and the fluid remains in the well-mixed regime. In the third case (the case we investigated this summer) the particle concentrations and inclination angles are large. This characterizes the ridged regime; the case in which the bulk velocity of the particles is faster than that of the liquid it is suspended in, resulting in a particle-rich ridge.

Our work focuses on experimentally analyzing the inclusion of surface tension in the model given by [6]. First, we looked at the existence of fingers; when part of the front separates into finger-like pieces leading the slurry down the track. Theoretically, this fingering instability is greatly dependent on surface tension. Then, we looked at two discontinuous shock solutions that are dependent on a thin precursor layer [5]. We focused on experimentally verifying the predicted shock formation. We compared the height profile of the ridge to numerical simulations under similar conditions to determine if these numerical results were legitimate physical solutions.

2 Theory

2.1 Mathematical model

The general mathematical model is based on the Navier-Stokes conservation of momentum equation for an incompressible fluid,

$$-\nabla \cdot \left(-P\mathbb{I} + \mu(\phi)(\nabla \mathbf{u} + \nabla \mathbf{u}^{\top})\right) = (\rho_p \phi + \rho_l(1-\phi))\,\mathbf{g}.$$

Here, we consider the particles and the oil together as a fluid. The coordinate plan for the system can be seen in the schematic diagram in Figure 4. We focus on the x- and z-directions as seen in the diagram below where the x-direction runs parallel to the incline and the z-direction is perpendicular to the plane. Also, note that $\mathbf{u}$ and $\mathbf{w}$ are the velocity terms for the x- and z-directions, respectively.

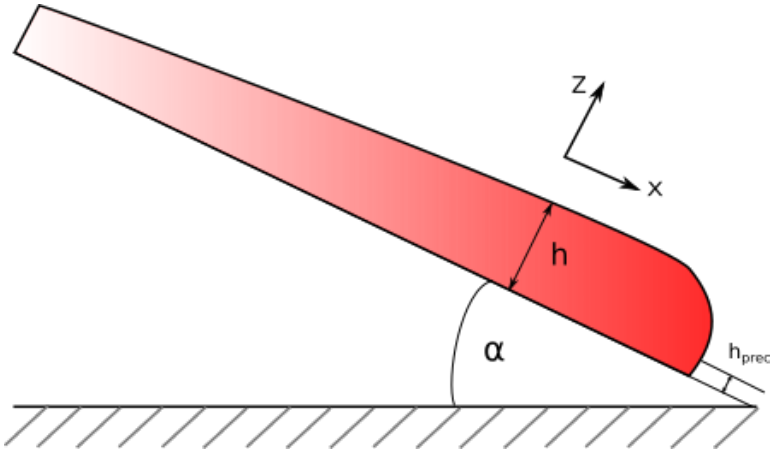

By dissolving the Navier Stokes equations down into components, we have:

$$\begin{aligned}
\rho(u_t + uu_x + wu_z) &= -p_x + \mu(u_{xx} + u_{zz}) + \rho g \sin\alpha \\
\rho(w_t + uw_x + ww_z) &= -p_z + \mu(w_{xx} + w_{zz}) - \rho g \cos\alpha \\
0 &= u_x + w_z.
\end{aligned}$$

The left side is known as the material or substantial derivative and this is balanced on the right by the pressure gradient, frictional term, and gravitational force. Lastly, the third equation is the condition for incompressible flow. The next step is to note that this type of system falls in a regime known as Stokes flow, which is characterized by a small Reynolds number given by

$$Re = \frac{UL}{\nu},$$

where U is the characteristic velocity, L is the length scale of the experiment, and ν is the kinematic viscosity. Since the velocity is relatively slow and the viscosity is very large with the viscous silicone oil, the flow is Stokes flow because $Re \ll 1$. This flow has interesting properties such as being considered 'reversible' (check this link out). Due to the low Reynolds

number, the material derivatives in the fluid equation are approximately zero, and our system reduces to

$$\begin{aligned} 0 &= -p_x + \mu(u_{xx} + u_{zz}) + \rho g \sin\alpha \\ 0 &= -p_z + \mu(w_{xx} + w_{zz}) - \rho g \cos\alpha \\ 0 &= u_x + w_z. \end{aligned}$$

Next, we can use the lubrication approximation, $\epsilon = H/L \ll 1$. This is because the height of the slurries is small compared to the length of the track,which is approximately a meter. This further simplifies the equations to the following,

$$\begin{aligned} 0 &= -p_x + (\mu u_z)_z + \rho g \sin\alpha \\ 0 &= -p_z - \rho g \cos\alpha \\ 0 &= u_x + w_z. \end{aligned}$$

From here the equations are tractable using numerical methods as long as we can apply boundary conditions. These are the kinematic condition: $\frac{\partial h}{\partial t} = w - u\frac{\partial h}{\partial x}$, at $z = h$, the stress balance condition: $p = p_{atm}$, at $z = h$ and $\mu u_z = 0$, at $z = h$, no through-flow condition: $w = 0$, at $z = 0$ and the no slip condition: $u = 0, w = 0$, at $z = 0$.

To standardize our model, we non-dimensionalize according to the scales below:

$$[x] = \frac{H}{\epsilon}, [z] = H, [\phi] = 1, [\mu] = \mu_l, [u] = \frac{H^2 p_l g \sin\alpha}{\mu_l} = U,$$

$$[w] = \epsilon[u], [t] = \frac{[x]}{[u]}, [J_z] = \frac{d^2[u]}{[z]^2}, [J_x] = \epsilon[J_z], [P] = \frac{[u][\mu]}{[z]},$$

where brackets define the characteristic size of the variable.

The second important equation of our model is the particle transport equation,

$$\partial_t \phi + \mathbf{u} \cdot \nabla\phi + \nabla \cdot \mathbf{J} = 0$$

where $\mathbf{J}$ is the flux and ϕ is the particle to liquid concentration. Now we can use the equilibrium assumption Equation 1, which can be applied since the distance the particle settles in the x-direction is asymptotically smaller than the lubrication scale, $[x]$. Also, the flux in the z-direction is at equilibrium so we can say the leading order is zero. From here, we look at the height, h, and integrated volume fraction, n, in the $x-$direction for the first order in the shock theory [4].

2.2 Shock Theory

As the fluid front moves in the x-direction, it evolves in the z-direction resulting in the formation of a shock. The hyperbolic conservation laws with Riemann initial data give rise

to the transport equations that describe this shock. The thickness of a precursor layer determines the type of shock predicted from the transport equations. When the precursor h_R is smaller than some critical thickness, the singular shock forms. It is characterized by the intermediate height in the shock layer being unbounded and growing in the z-direction, which happens as the particle concentration ϕ approaches ϕ_{max}.

First order transport equations are given as:

$$\begin{aligned} 0 &= h_t + (h^3 f(\phi))_z \\ 0 &= n_t + (h^3 g(\phi))_x \end{aligned}$$

where $f(\phi)$ and $g(\phi)$ are are fluxes that depend on the equilibrium solutions for the particles. These have the Jacobian

$$J = h^2 \begin{bmatrix} 3f - \phi_0 f' & f' \\ 3g - \phi_0 g' & g' \end{bmatrix}$$

and determinant

$$\mathcal{D} = (3f - \phi_0 f' + g')^2 - 12(fg' - fg').$$

This guarantees hyperbolicity of the system given $\mathcal{D} > 0$.

If surface tension, which is zero in the first order equations, is retained we arrive at the fourth order equations:

$$\begin{aligned} h_t + \left(h^3 f\right)_x &= -\beta \left(h^3 f_1 h_{xxx}\right)_x \\ (h\phi_0)_t + \left(h^3 g\right)_x &= -\beta \left(h^3 g_1 h_{xxx}\right)_x, \end{aligned}$$

where the integrated volume fraction, n, is

$$n(x,t) \equiv \textstyle\int_0^h \phi \, dz.$$

These equations include a term for degenerate diffusion to model surface tension with a physical parameter, β, to adjust according to the dominance of surface tension. Solutions to these fourth order equations are dependent on the precursor height which ultimately dictates which type of shock solution to the transport system occurs [5].

Classic shock solutions are found for $\phi_R = \phi_L$. In the system we are focusing on, a hyperbolic system with Riemann initial data, this appears as

$$h(0,x) = \begin{cases} h_L, & x < 0 \\ h_R, & x > 0 \end{cases}, \; \phi_0 = \begin{cases} \phi_L, & x < 0 \\ \phi_R, & x > 0 \end{cases}, \; n(0,x) = h(0,x)\phi_0(0,x)$$

where h_L and ϕ_L denote the height of the mixture and particle concentration for the reservoir respectively. h_R and ϕ_R correspond to the precursor similarly.

Shock solutions differ depending on the height of the precursor layer as a fraction of slurry height. The model predicts the formation of a singular shock for a precursor height of $h_R \lesssim 0.05 h_L$. A shock solution would be given by

$$h(t,x) = \begin{cases} h_L & x < st \\ h_R & x > st \end{cases}$$

where s is

$$s = \frac{(h_L^2 + h_R^2 + h_L h_R)(\phi_{max} f(\phi_L) - g(\phi_L))}{\phi_{max} - \phi_L}.$$

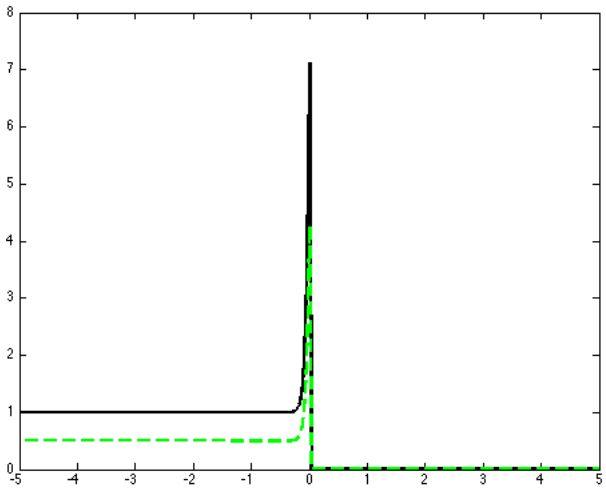

Figure 1: Singular shock

In the first order case this shock resembles a delta function as seen in Figure 1. A singularity is not observed in experimentation because surface tension is nonzero and normal gravity smooths this feature. The fourth order equation which accounts for these physical effects gives a singular shock solution that is characterized by an increase in height and thinning of the ridge as it moves down the plane [5].

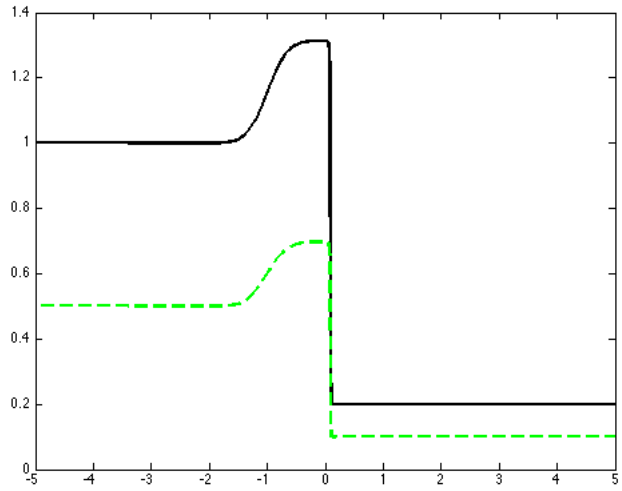

Figure 2: Double shock

The model predicts the formation of a double shock for $\phi_L > \phi_{crit}$, or when the precursor height is sufficiently large $h_R \approx 0.1 h_L$. This appears in Figure 2 as a widening of the leading particle ridge. Similar to the singular shock, the first order solutions differ from the fourth order solutions and the physical solution because of the smoothing of surface tension and normal gravity.

2.3 Numerical Methods

The numerical method used for the theory is a finite difference method. The nonlinear part is explicit and the linear part is treated implicitly. To solve the first order system mentioned above in the shock theory section an upwind method [2] is employed. To perform the numerical simulation, a MATLAB script (named `Full_ST2_moving_singular.m`) is run with `mat` files that contain `PxLarge`, `PxNeg`, `PxSM`, and the angle of the experiment in their titles. These files are computed using a separate code written by Li Wang. The `Px` value varies depending on the size of the fourth order term. These `mat` files are the fastest to use, otherwise `compute_fluxes_ST.m` and `fff_ST2.m` will need to be in the same directory as `Full_ST2_moving_singular.m` and the code will take a much longer time to run due to the extra requisite computations.

In the `Full_ST2_moving_singular.m` script, the parameters `PHI0`, `angle`, `V`, `rhopart`, and `rholiq` must be changed to match the parameters of the target experiment. One parameter that can be changed if desired is the thickness of the precursor height, `precc`. Note that altering this size may cause problems with the CFL condition and you may see the error message:

```
Error using Full_ST2_moving_singular (line 276)
A is NaN
```

At line 323, the variable dt can be made smaller by making the denominator larger than 5. This may fix the issue, however the last resort would be to set beta equal to 0 in order to remove the fourth order surface tension term all together. Then there would be no CFL condition to worry about. To do this, beta should be set to zero before the while loop, so uncomment the line 105 after the speed is set to zero.

The next thing to set is tFinal which can be determined by nondimensionlizing the final time seen in the experiment. First, calculate the variables U and L by using,

$$L = \left(\frac{\gamma H_0}{\beta \rho_l g \sin \alpha} \right)^{1/3}, \; U = \frac{H_0^2 \rho_l g \sin \alpha}{\mu_l}$$

where $H_0 = 0.01$, $\beta = 0.01$, and $\gamma = 0.02$. This calculation should already be present in the code. Then take the final time seen in the experiment and multiply it by U/L to nondimensionalize it. This should be set to tFinal, and the TIME variable set in the code should be an array which does not extend past that nondimensionlized final time. Lastly, the filename string on the last line should be named uniquely, and preferably according to the chosen parameters.

The results of the numerical simulation can then be nondimensionalized. From the saved mat file, load the following variables: L, U, x, HH, and TIME. Then run the following conversion:

```
X = L*x*1e2;  %cm
H = HH*H_0*1e3; %mm
time = TIME * L/U;
```

X is now the position along the track in centimeters. H is the height in millimeters with rows that correspond to the time in seconds listed in the time array.

3 Experimental Procedure

3.1 General Setup

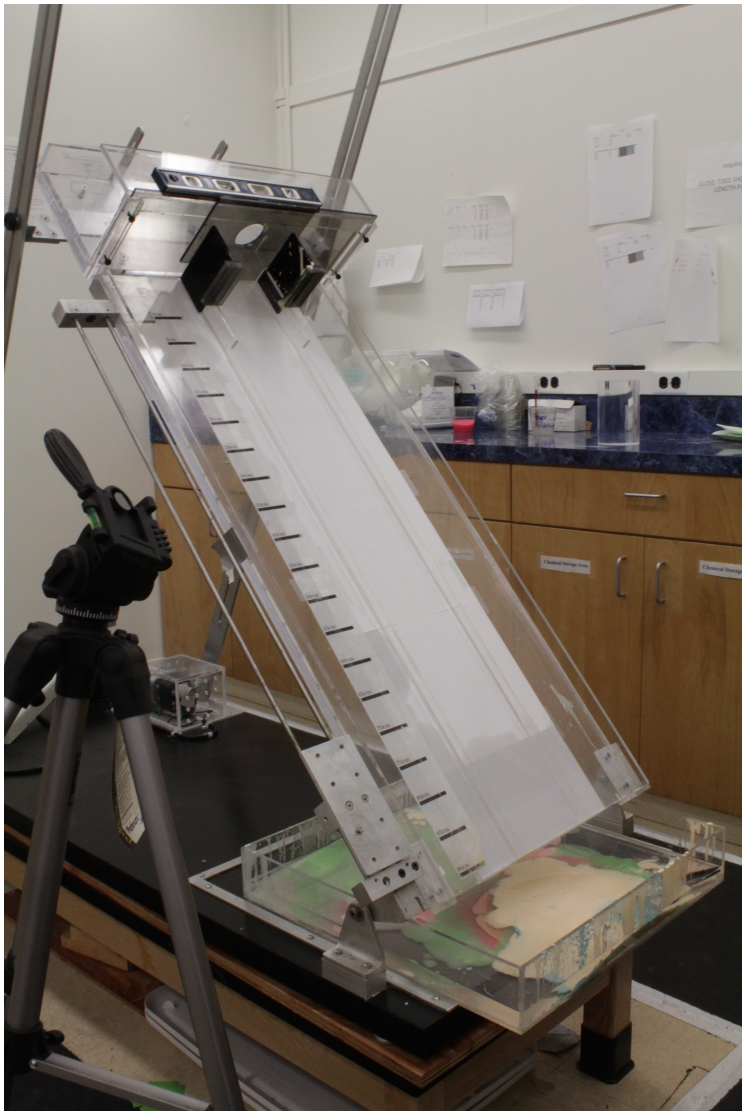

Figure 3: General setup

Our experimental apparatus is housed in the Applied Mathematics Laboratory at the University of California Los Angeles (UCLA). The setup is an acrylic inclined plane set on a platform with an adjustable angle (α). The plane serves as the surface on which the particle-laden slurries flow due to gravity. The slurries are made using differing concentrations of silicone oil and either glass (GSB) or ceramic (SLZ) particles. Each experiment begins by selecting the desired angle, particle, particle volume fraction (ϕ), volume of the slurry (V), and diameter of the particle (d).

We set the x-axis as the slope of the plane, and the z-axis in the normal direction. The y-axis points in the transverse direction along the width of the track. This direction is ignored for simplicity in the model. A schematic diagram of this setup can be seen in Figure 4. The dimensions of the gate in which the slurry is loaded are 5 cm by 14 cm and the dimensions of the track on which the slurry flows down are 90 cm by 14 cm.

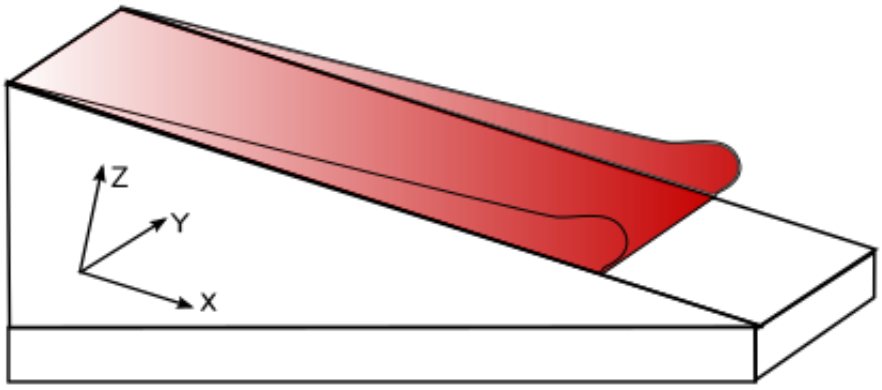

Figure 4: Schematic diagram of inclined plane

3.1.1 Experiment Specifications

Multiple variations of silicone oil and particles are available for use in the lab. In our experiments we use 1000 cSt oil and three different diameters of both glass and ceramic particles, denoted by the number following the type of particle. Note that for glass particles a higher number implies a smaller diameter, whereas for the ceramic particles a higher number implies a larger particle. The exact specifications are given below.

Particle Type (Glass)	Diameter Range (mm)	Particle Type (Ceramic)	Diameter Range (mm)
GSB9	0.150-0.180	SLZ1	0.07-0.125
GSB7	0.180-0.250	SLZ2	0.125-0.250
GSB5	0.20-0.425	SLZ3	0.250-0.425

When choosing the parameters for an experiment, we insure that all model assumptions are met so that we can compare our experimental results to theoretical predictions. Two important inequalities to check when fixing parameters for an experiment are the continuum assumption,

$$\left(\frac{d}{H}\right)^2 << 1,$$

and equilibrium assumption,

$$H\left(\frac{d}{H}\right)^{-2} \frac{18\rho_l}{\rho_p - \rho_l} \tan(\alpha) << \frac{H}{\epsilon}, \tag{1}$$

where ρ_p and ρ_l are the densities of the particle and oil respectively. Since our track is $\approx$ 1 m in length, we use $\epsilon = 6 \times 10^{-4}$ [4]. These inequalities determine the volume scales that we can use for each combination of parameters.

For both the fingering instability and height profile experiments, we are mainly interested in the dynamics of the slurry in the ridged regime. Therefore, for all experiments we select combinations of parameters that will result in the particle-laden fluid evolving into a well defined ridge leading the front.

3.2 Particle Dyeing

We dye the particles for aesthetic reasons as well as to determine regions of high particle concentration. Dying the particles can also help us easily differentiate between different particle types. The ceramic particles used in experiments are initially white in color, and can be dyed with food coloring. To dye the particles, we use approximately 20 drops of food coloring for every 400 g of particles. The particles are then placed in a Zip-Lock bag, which is then sealed and thoroughly mixed until the color appears uniform. The particles are given an adequate time to absorb dye and dry before they are used in any experiments.

The glass particles used in experiments are initially transparent, and can be dyed with acrylic paint. To dye the particles, 5 mL of acrylic paint and 5 mL of water are added into a beaker and thoroughly stirred. The mixture is then poured into a Zip-Lock bag with the particles and allowed to mix and dry. If darker colors are desired, more dye can be added as necessary.

Particle clumping can result in a nonuniform distribution of particles that may affect the dynamics of the slurry, most noticeably in the ridge. This issue can be resolved by leaving the particles spread out in a paper plate for a day and mixing/grinding them in another clean Zip-Lock bag until no observable clumps are remaining.

3.3 Pre-layering

Pre-layering or 'pre-wetting' is our term for applying a uniform thin film of oil on the track before the slurry is uploaded to the gate. This additional layer of oil is applied in order to avoid an additional consequence of contact line physics of where the particle-laden fluid meets the acrylic track. With our pre-layering technique, the slurry instead flows down the thin layer of oil above the acrylic track. An important consequence of this is that we can now justify using the lubrication approximation in our model, thus greatly reducing the model's complexity. We have also observed that pre-wetting the surface has reduced the prevalence of the fingering instability, explained further in Section 3.5.

The track is first wiped down and cleaned thoroughly of any remnants of the last experiment. To pre-wet the track, we then pour approximately 20 mL of 100 sCt oil into the

gate and let it flow freely down the track. The less viscous oil is used because it is a good medium to both lubricate the acrylic and also allow the slurry to flow uninhibited down the track. We then use a small squeegee device to spread the oil evenly and thinly throughout the plane. Additional care should be taken at the boundary walls of the track to ensure that the oil is uniformly thin.

An additional way to pre-layer the track is to pour fluid down the slope and leave it for a sufficiently long time (depending on the angle of inclination) to run down the track and become approximately uniformly thin. However, this technique was never used because it time expensive and requires the track to be extremely clean before it is implemented.

3.4 Mixing and Volume Procedures

To create the slurry, we mix together the specified particle and oil mass based on the particle volume fraction and total volume. We use a MATLAB program to generate a spreadsheet that allows us to easily determine the required masses of particle and oil to make up the slurry given a ϕ and V value. The required amounts are measured separately in cups, and then the particle cup is poured into the oil cup to limit the amount of volume lost. Next, we stir the mixture vigorously with a spoon or other stirring device to reduce air bubbles. The cup containing the slurry can also be gently hit against a hard surface to help get rid of any hard to reach bubbles. Finally the particle-laden fluid is mixed slowly to thoroughly mix the particles and oil together.

Once the slurry is well mixed, it should be immediately loaded into the gate to avoid settling. While loading the slurry, care must be taken to not let any slurry fall onto the track. It can be extremely difficult to load the entire volume of the slurry into the gate. The reasons are trifold: the slurry must be uploaded quickly to avoid resettling, the slurry is viscous and sticks to the cup, and the gate is small with high walls. Also, the gate becomes increasingly difficult to load as the angle of the track increases. This results in a significant amount of slurry being left behind and lost. To estimate this volume lost, we determine the mass of the slurry that was left behind in the cup. This can then be used to calculate the percentage of mass lost, which can then in turn be used to calculate the percent and amount of volume lost.

3.5 Finger Instability Experiment

The fingering instability refers to the regime in which the front of the slurry becomes non-uniform and evolves into a finger profile as it moves down the track. A picture of this can be seen in Figure 5. We are interested in the fingering instability phenomena and how it relates to the particle diameter and angle of inclination.

Figure 5: Fingering picture of GSB7 at $\phi = 0.45$, $\alpha = 70°$, and volume = 110 mL

We conducted fingering instability experiments at sequences of different angles with different sized particles. During each experiment, we would manually take pictures of the front with a Cannon Rebel T3 camera. These were then uploaded onto a shared hard drive for analysis. Each experimental detail was recorded carefully and then organized on a spreadsheet that included the specified angle/size, pictures of the experiment, the number of fingers, and the ϕ_{finger} concentration which will be expanded upon in the next section.

One difficulty we had with these experiments was a clear way in which to document how many fingers had formed. It was common for the slurry to form a couple of defined fingers and then a couple of partially defined atypical fingers. We determined that each partial finger would be estimated against an actual finger and would be counted as whatever fraction of a finger was appropriate. The results of these experiments are in 4.1.

3.5.1 Measuring Finger Concentration

During the fingering instability experiments, we became interested in how the particle volume fraction at the finger (ϕ_{finger}) compared to the particle volume fraction initially (ϕ_{inital}). In the theoretical model, the particle-rich ridge would continue to increase until it reach the maximum packing fraction (ϕ_{max}). Experimentally, we observe that the ridge appears to become increasing saturated until it either flows completely down the track or 'breaks'and falls down the remainder of the track. While this breaking is not predicted by our numerical model, it is reasonable to hypothesize that the ridge will break when it reaches ϕ_{max}. Recent estimates place $\phi_{max} \approx 0.61$ [4].

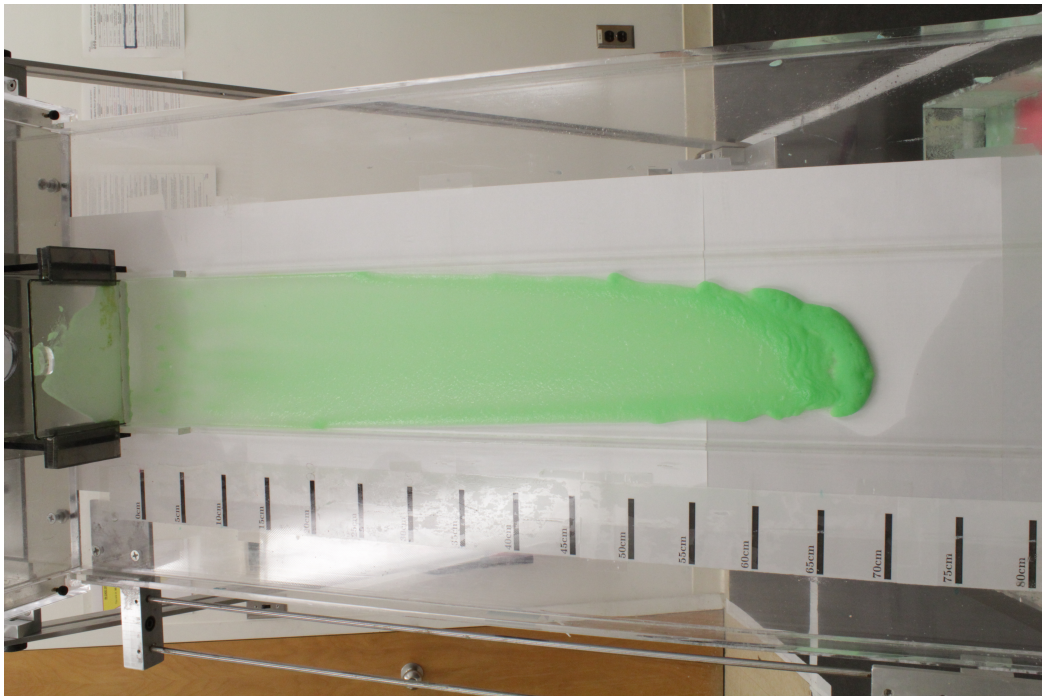

Figure 6: GSB7 at $\phi = .45, \alpha = 60°, V = 110\,\text{mL}$ in the process of breaking

We devised an expensive way to measure ϕ_{finger}. When the ridge starts to crack, it generally takes around five seconds to completely break and fall down the track. It is during this interval that we use a clean squeege to completely cut off one or more fingers from the slurry. We then squeege this down the track into a plastic 10 mL graduated cylinder. The contents of the slurry are then pushed to the bottom of the cylinder and stirred to reduce air bubbles. The cylinder can also be hit gently against a hard surface in order to further reduce air bubbles. The cylinder is then labeled and left to sit out overnight in order for the particles and oil to separate, thus further reducing the amount of air bubbles. Once this has occurred, we can measure the mass and volume of the cylinder. Using the previously known densities of the oil (ρ_l) and particles (ρ_p), we can use

$$\rho_p \phi + \rho_l (1 - \phi) = \frac{M}{V}$$

to calculate ϕ_{finger}. The results of these experiments are in 4.2.

3.6 Finger Growth Experiments

Finger growth experiments were conducted to determine if there was a critical angle in which the fingers stopped growing after they had formed during the transient stage (discussed in Section 3.6.1). We tested this hypothesis by fixing all parameters other than the angle of inclination. We ran three experiments at five different angles and then calculated

the observed and theoretical transient length of the slurry, the number of fingers, and the average length of the fingers at the end of the transient stage and at the end of the track. The length of the finger was calculated twice: at the observed transient length and just before the slurry either broke or ran out of the frame, depending on which happened first. The length of the finger was defined as the distance from the tip of each finger to the part of the front it connected to. Growth was calculated as the difference in length from the two measurements. This procedure was designed to be a quantitative way to measure and analyze the dynamics of the fingers compared to the dynamics of the front. The results of these experiments are in 4.3.

3.6.1 Transient Length

The transient length refers to the length of the track in which the slurry stays in the well-mixed regime, where the particles and oil flow at approximately the same rate. All of our experiments were in the ridged regime, so the transient stage was complete when a clear ridge had formed on the track. This can be very difficult to precisely determine experimentally because of the slow onset of the ridge. Generally, we observed the transient stage ending over a range of 10 cm and we set the transient length as the middle of that range. Theoretically, we have approximate formulas to calculate the transient length given in [4] and [1].

3.7 Height Profile

We also conducted height profile experiments in order to determine the profile of the front as it moves down the track. These experiments were conducted with a goal of comparing and testing the double and single shock solutions given by [5]. The double and single shock solutions will be expanded upon in Section 4.4. For the height profile experiments, we fan a green class II laser down the track from above as seen in Figure 7. The laser shines through the acrylic sheet, but reflects off of the slurry, giving us a height profile of the slurry. The camera is setup in a fixed position in order to capture the experiment as it progresses. The primary parameter varied was volume because the volume changes the effective precursor height which theoretically determines whether the height profile will form a double or single shock. Other variables adjusted included the inclination angle and particle concentration.

Figure 7: Experimental setup for the height profile experiments. The camera and laser are in position to capture the height profile of the slurry. During the actual experiment the lights would be turned off.

The initial experiment ends when the slurry stops, breaks, or flows off the track. We then must determine the calibration for the current placement of the camera and laser. First, the track must be completely cleaned of the slurry. This can be done by squeeging off the track and wiping it down with a paper towel. We then take three sets of photographs for calibration: plain track, paper, and quarter stacks. The plain track photograph is a picture of the completely clean track. The paper photograph is a picture of a long piece of white paper laid flat on the track covering the entire camera frame. The quarter stacks photographs are pictures of a stack of three quarters moved down the track at every 2.5 cm throughout the camera frame. This can be seen in Figure 8. Both the plain piece of paper and quarters have a known thickness that can then be used in our MATLAB code to calibrate each experiment. This calibration process will be further explain in Section 3.7.1.

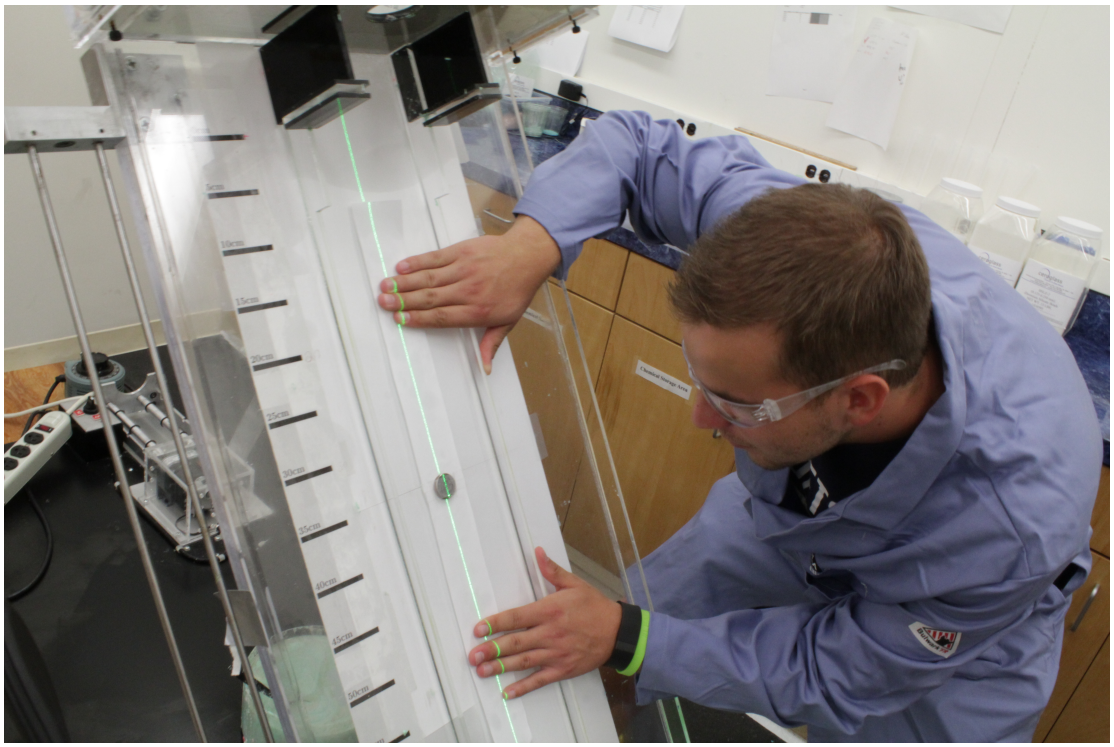

Figure 8: Quarter calibration shots, taken every 2.5 cm over a specified range

The final step to complete before image processing is the documentation of the details of each experiment. We record the pertinent information from an experiment on a text file and save it in the same folder as the experimental data and results. This was especially important as we completed a high quantity of experiments. An example note is shown in Figure 9.

```
SLZ3
size: 0.25-0.425 mm
density: 3.80 g/cm^3
volume 110 mL, remainder: 18.9g
actual volume:  101.58mL
concentration = 0.45 (1,000 cSt oil mass: 58.7g, particle mass: 188.1g)
pre-lube w/ 100 cst
angle: 45


laser line used
line zero calibration shot
quarter calibration shots every 2.5 cm from 15-60cm



ISO 1600, F10, ss 1/25

Comments:
ridge losing volume to adjacent finger
broke at 60cm

Jkregs 7/20/2015

```

Figure 9: An example note which would be found in an experimental folder file. In the folder would also be the experimental pictures, calibration photos, and photos of the slurry.

3.7.1 Post-processing

The data we collect from our height profile experiments is a time series of raw JPG images of the laser line on our experimental apparatus. Since we run our experiments with external light sources as minimal as possible, the images have high enough contrast such that we can extract the approximate line of the laser in the image, which can then be scaled using our calibration process to the actual height of the fluid on the track.

Given the set of images, we first choose a cutoff brightness (typically 15 out of 255) and then get a matrix corresponding to each pixel where each value is either one or zero depending on whether or not it is above the cutoff. We then choose the median pixel in each column of the image that has a value of one, and from this extract an array of pixel heights. We then extract the same line from a reference image of the laser line on the blank track, and use this to find how much (in pixels) the lines from the experimental images deviate from the reference line.

As mentioned previously, we calibrate our image processing pipeline by placing an object of known height (in our case a stack of quarters) under the laser line at several locations along the track. We also take an image of the laser line on a blank piece of paper laid flat on the track in order to obtain the zero-height. Assuming that the horizontal plane of the camera is parallel to the plane of the track, these images allow us to easily calibrate the vertical and horizontal scaling factors and convert from pixel distances extracted from the

images to actual metric distances. Sample images obtained from various stages during our images processing are shown in Figure 10. Also shown is a plot from the final extracted line which we use for comparison to the numerical results.

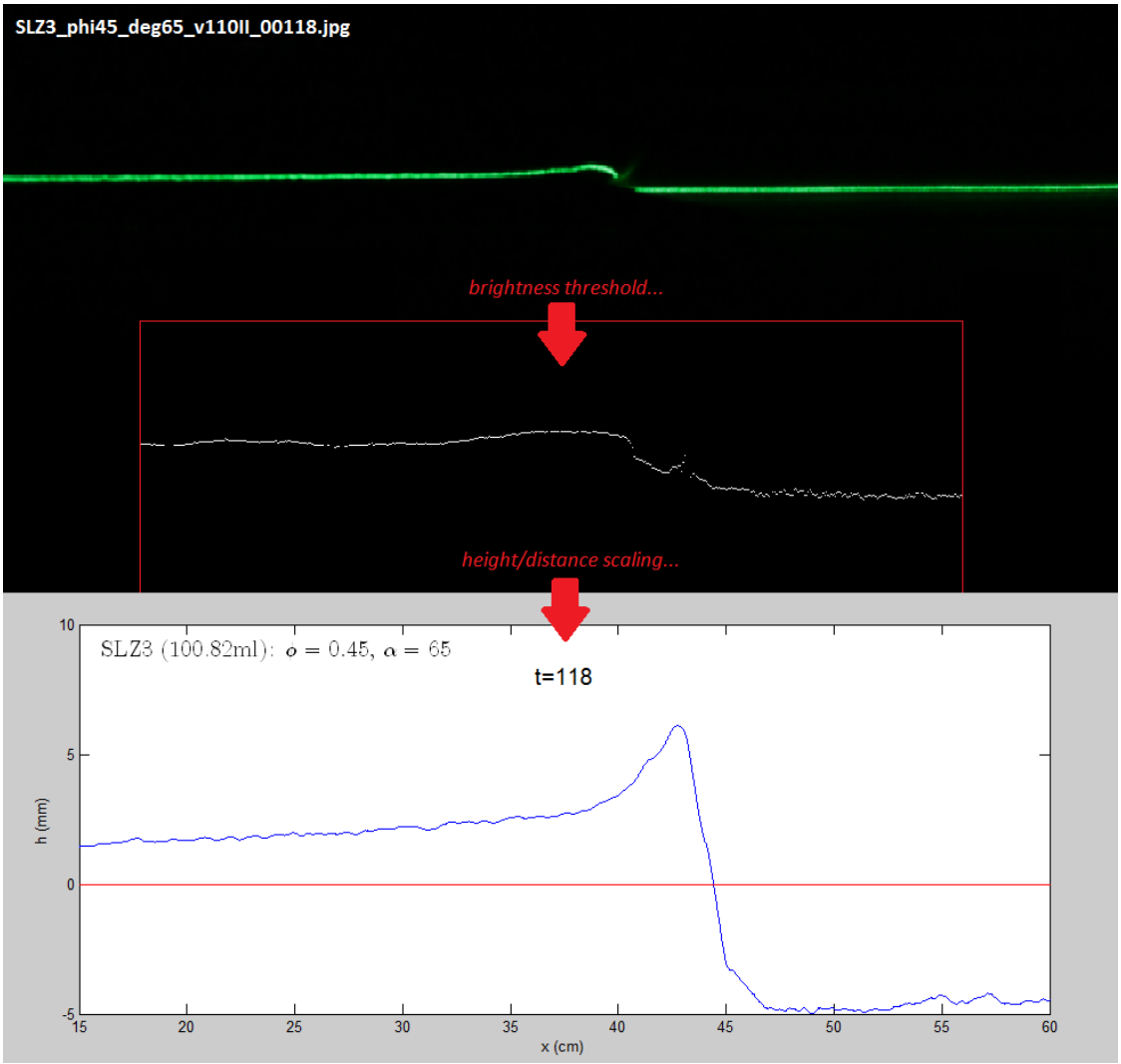

Figure 10: Example images from various stages of our post-processing pipeline. The top pane is a raw image taken during the experiment, and below it is a processed image with the laser line refined. The final pane is a plot of the extracted height profile. The red line represents the calibrated zero height, where the height profile in blue is the scaled deviation from that line. The height profile is below zero after the shock front because our actual track is made out of transparent acrylic. We calculate that the laser line should appear to be about 4 ± 0.2mm below the zero line due to refraction.

3.7.2 Difficulties

Over the course of building our image processing pipeline, we experienced several complications with regards to the quality of our experimental and calibration images. For the calibration we initially used a single quarter, but we found that our process was not sensitive

enough so we instead used a stack of three quarters which provided more consistent calibration results. Additionally, we experienced a problem where the laser line would be obstructed in the image. This can happen when the laser line falls on the opposite side of the target finger thus partially blocking it from the camera, or when at certain angles the track reflects laser light onto the finger, which can be seen in Figure 10. Unfortunately this will cause noise in our extracted lines, however we can sometimes use the surrounding frames to smooth the noise, and for the purposes of comparing height profiles we are usually able to capture the majority of the profile line. In general, especially as we have become more consistent with our experimental procedure, this kind of inconsistency in the data has only been a minor setback.

Other issues with shock data involves the placement of the laser line. We placed the line such that it was visible and in focus for the camera with disregard for where the fingers formed because they are unpredictable. It is clear in the two dimensional numerical model that the shock looks different from where it is viewed: matched up with the finger, alongside the finger, or on the lagging ridge.

4 Results

4.1 Finger Instability

As mentioned in 3.5, we became interested in how the particle size and the angle of inclination affects the fingering instability. Our results suggest that smaller particle size and higher angles of inclination result in a higher quantity of fingers. A demonstration of higher angles resulting in a higher number of fingers can be seen in Figure 11. In the experiments shown in the Figure, the particle type and particle volume fraction were kept constant while the angle was varied. At 50° the slurry formed 2 fingers. At 60° the slurry formed 3 fingers. At 70° the slurry formed what appears to be between 3 and 4 fingers.

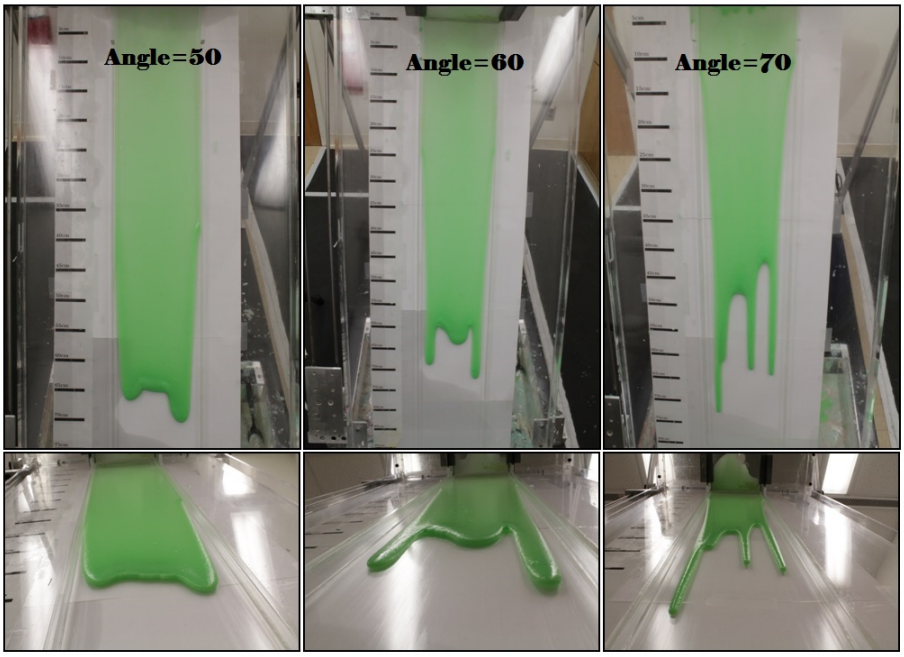

Figure 11: GSB9 at $\phi = 0.45$ at a selection of three different angles. The above pictures are taken at a normal angle to the track and the below pictures are taken from the bottom of the track looking upwards. All pictures were taken when the slurry was at approximately 65 cm down the track.

Our full results showing the correlation between particle size/angle and number of fingers can be seen in Figure 12. This figure shows that higher angles and smaller particles, which corresponds to the upper right region of the graph, generally result in a higher number of fingers.

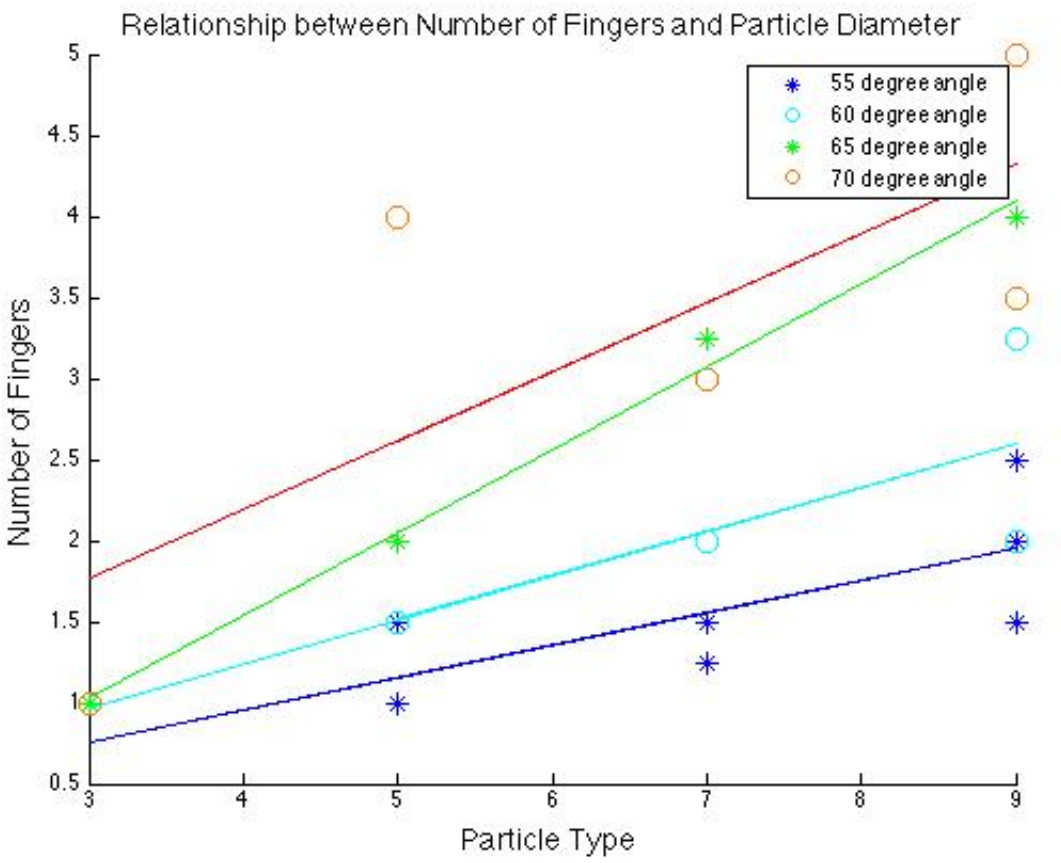

Figure 12: The relationship between number of fingers and particle diameter over a selection of angles. Note that for glass particles, as the number of the particle type increases the particle diameter decreases.

Higher angles resulting in a higher quantities of fingers is a trend that is consistent with other experimental and theoretical results in our field. The number of fingers is usually found to be dependent on the angle of inclination and the concentration of the particle-laden fluid. In our case, we believe that the higher the angle, the greater the effect of surface tension on the fingering instability, which results in more fingers. The effects of surface tension on our model are detailed in [2].

Smaller particle diameter resulting in a higher quantities of fingers is a novel result that our current model cannot account for. In the model, the only effect diameter has is on the particle flux, which eventually gets scaled out. Thus according to the model, the particle diameter (assuming it falls in the appropriate range for all model assumptions) should not have any effect on the evolution of the slurry.

4.2 Finger Concentration

We measured ϕ_{finger} concentrations on a limited number of experiments done when $\phi_{initial} = 0.45$ and $V = 110\,\text{mL}$. For these experiments, we varied the angle of inclination and the size of the particle. For each experiment $\phi_{initial} < \phi_{finger} < \phi_{max}$, which suggests that our experimental procedure was overall successful and realistic. Due to the limited number of experiments, there was no clear correlations in the data we obtained. However, one trend that was observed was that higher angles could sometimes result in very long fingers that would result in a lower ϕ_{finger} concentration. This is because long fingers are often comprised of higher oil concentrations then short, fat fingers that are just a ridge of particles. Our experimental procedure was to take the whole finger for measurement, which resulted in taking much more oil in the longer fingers. This could have been a cause for lower ϕ_{finger} values for higher angles. Our results are shown in Figure 13.

Particle	Angle	Finger phi
GSB9	55	.58
GSB7	55	.53
GSB5	55	.57
Average		***.56***
GSB9	60	.52
GSB9	60	.58
Average		***.55***
GSB9	65	.52
GSB7	65	.54
GSB5	65	.57
Average		***.54***
GSB9	70	.52
GSB7	70	.52
Average		***.52***

Figure 13: ϕ_{finger} experimental data. All trials were conducted at $\phi_{initial} = 0.45$ and $V = 110\,\text{mL}$. Initial trends suggest that as angle increases, ϕ_{finger} decreases.

4.3 Finger Growth Experiments

We observe that at large angles the fingers move faster down the incline than at small angles. These fingers tend to grow longer and thinner. At lower angles, we observed that once a finger is formed, it seems to move at the same speed as the front, thus staying at a constant length, or in rare cases, shrinking into the front. This idea can be seen in Figure 14. The fingers of the higher 70° angle slurry grow much longer after the transient stage then the fingers of the lower 60° angle slurry.

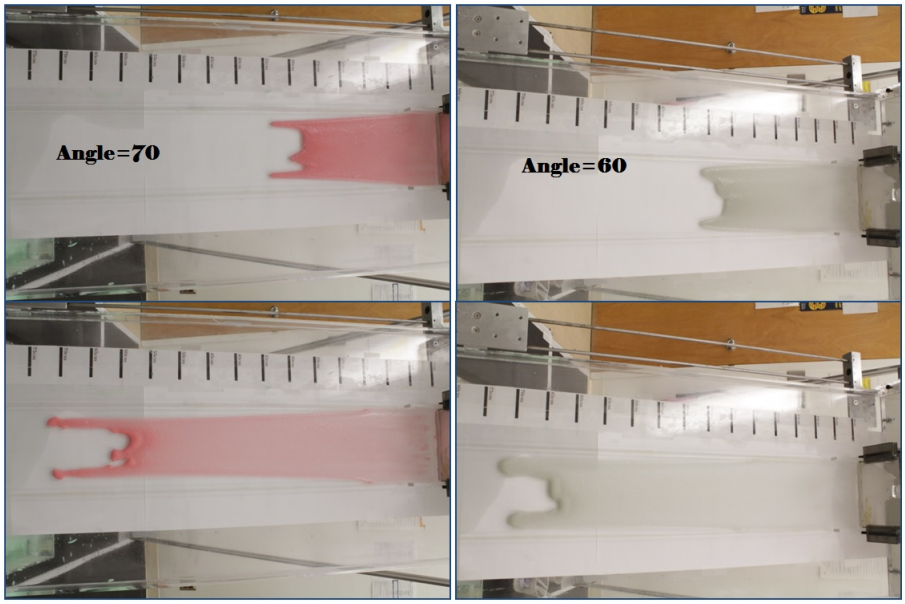

Figure 14: GSB7 at $\phi = 0.45, V = 110\,\text{mL}$. The left red slurry is at $\alpha = 70°$, whereas the right silver slurry is at $\alpha = 60°$. The top pictures were taken near the end of the transient stage and the bottom pictures were taken when the slurry stopped/broke.

This trend can be further examined in Figure 15. Here, we see a positive correlation between angle and finger growth.

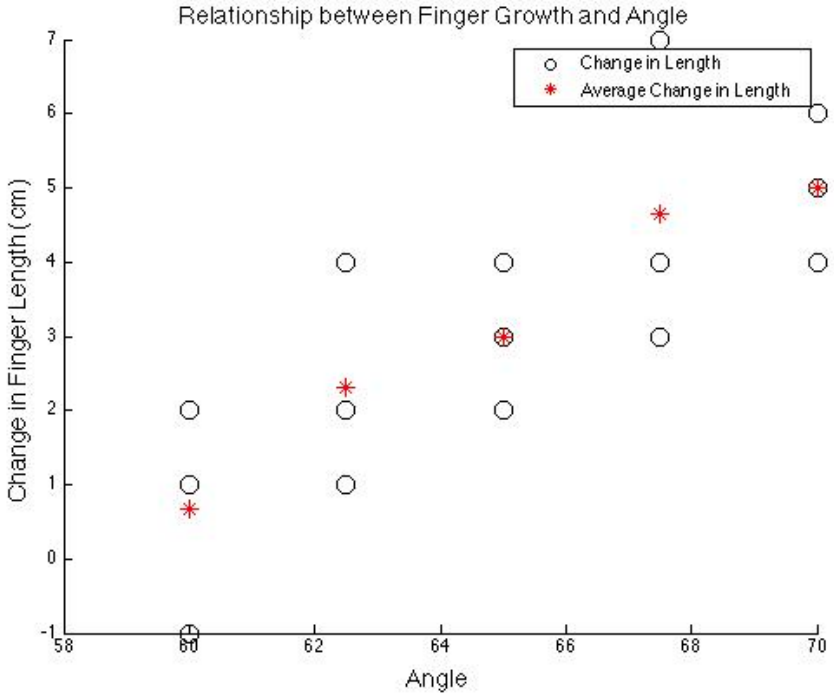

Figure 15: The relationship between the growth of fingers and the angle of the inclination. All experiments were conducted with GSB7 at $\phi = 0.45, V = 110\,\text{mL}$

4.4 Height Profile

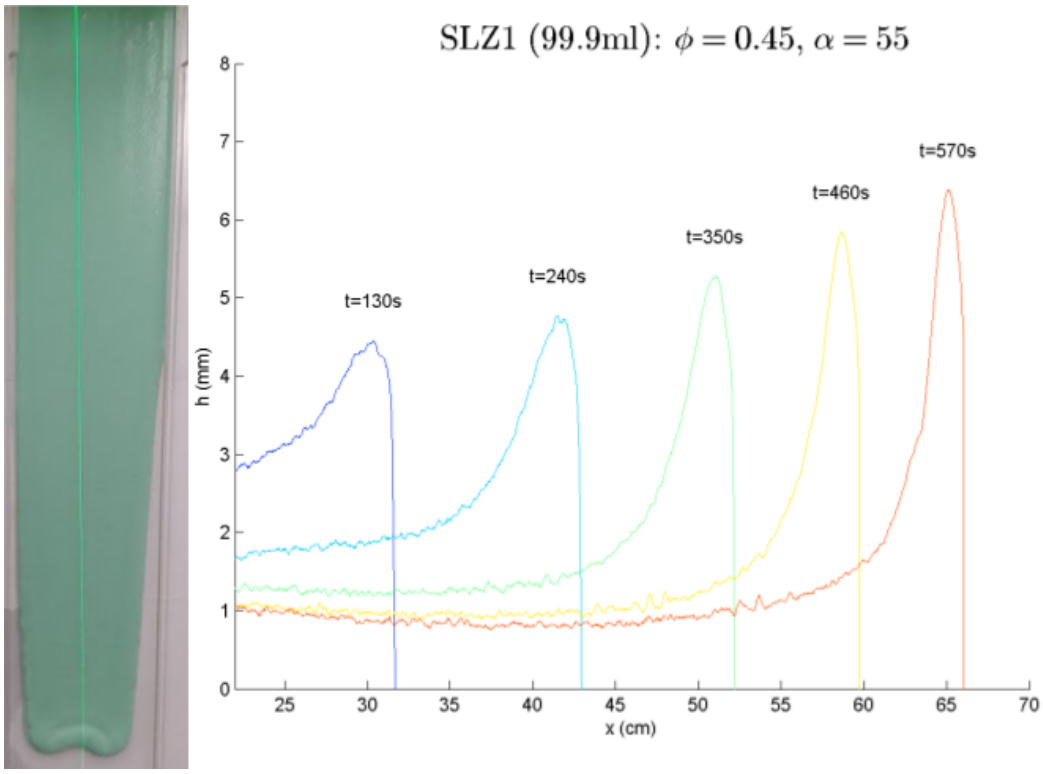

Figure 16: Picture of the laser line location (left), processed experimental height profile over time (right)

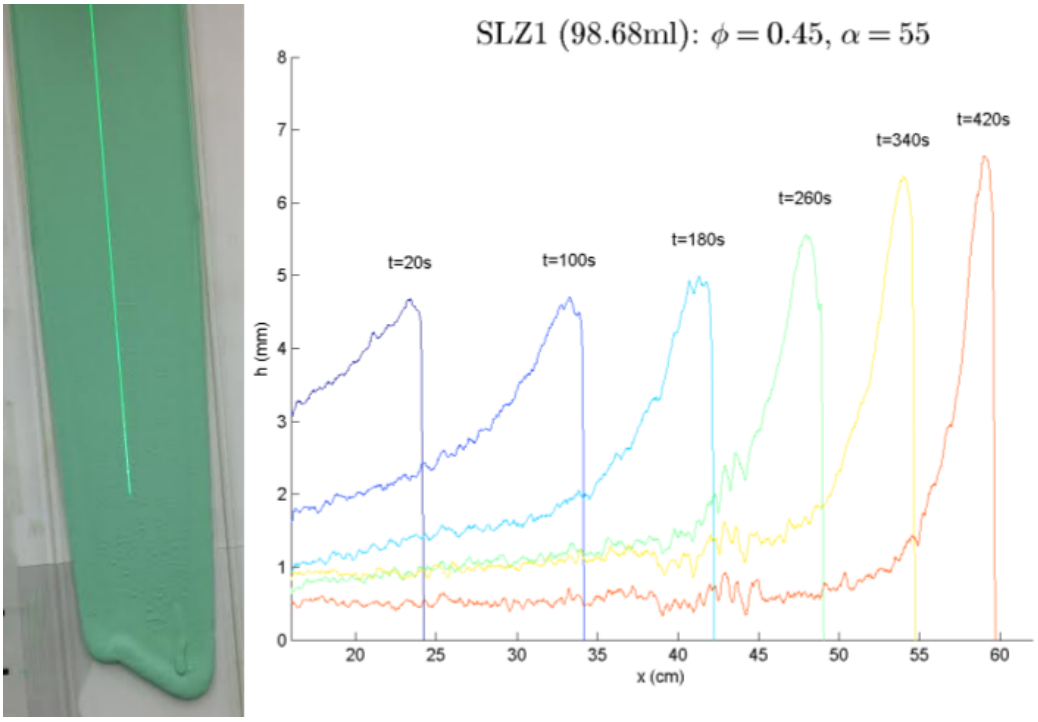

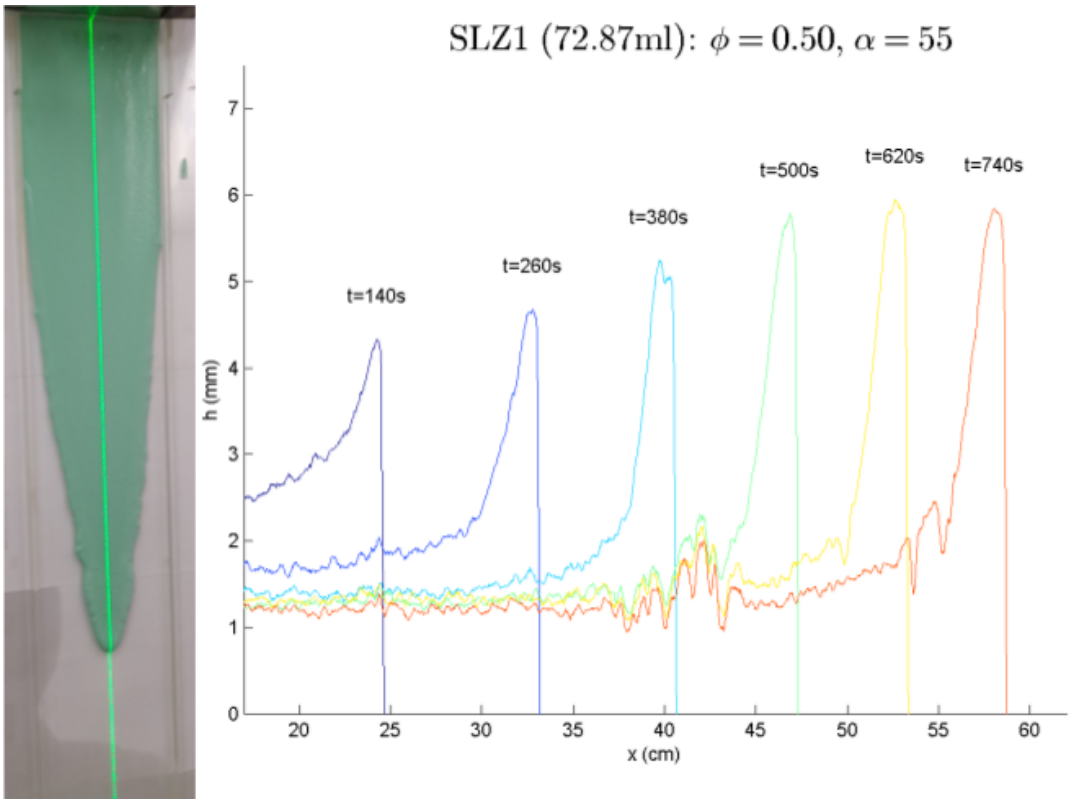
SLZ1 (72.87ml): $\phi = 0.50$, $\alpha = 55$
t=140s
t=260s
t=380s
t=500s
t=620s
t=740s
h (mm)
x (cm)

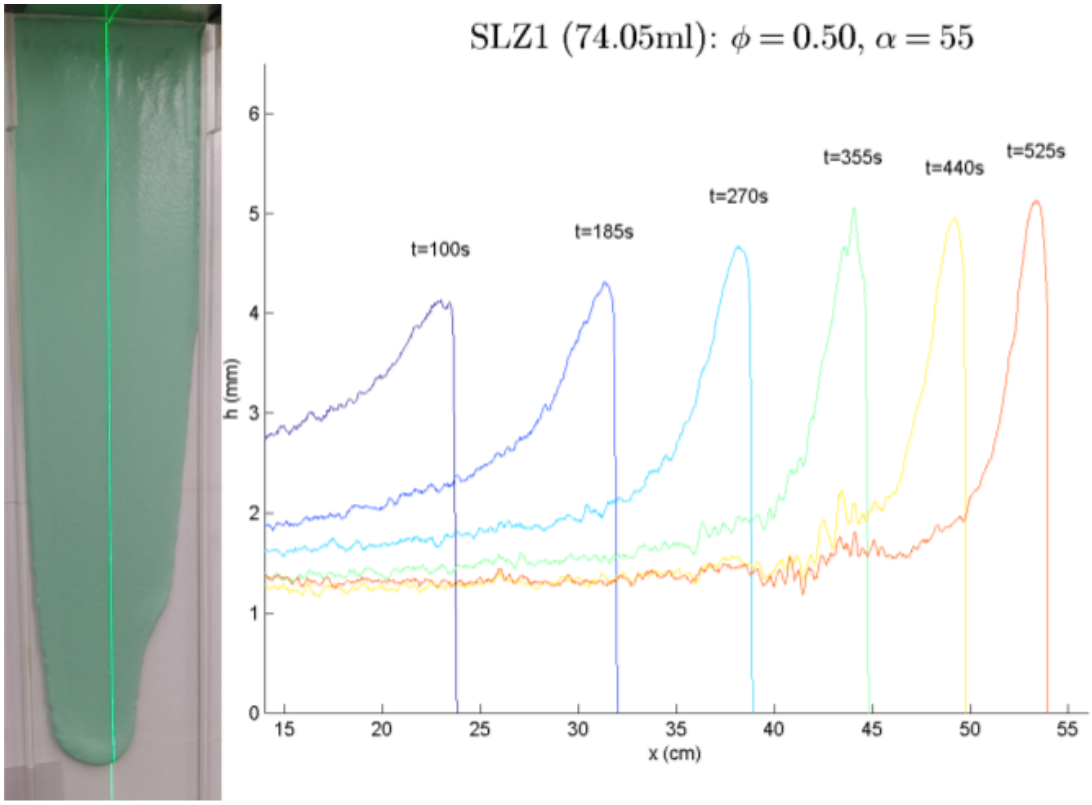
SLZ1 (74.05ml): $\phi = 0.50$, $\alpha = 55$
t=100s
t=185s
t=270s
t=355s
t=440s
t=525s
h (mm)
x (cm)

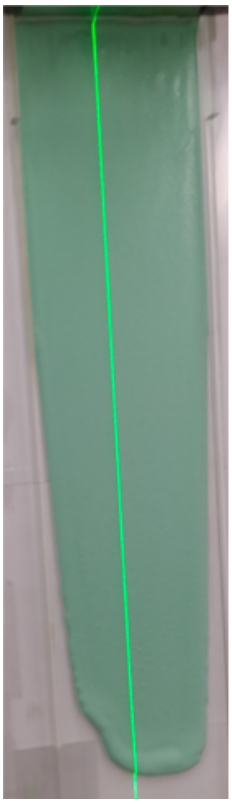

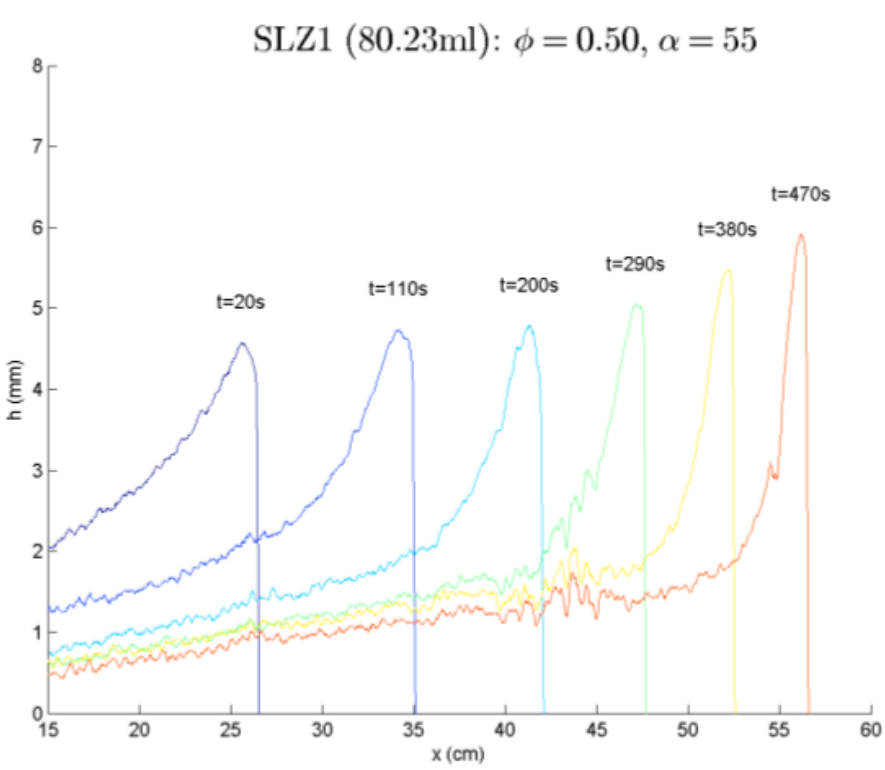
SLZ1 (80.23ml): $\phi = 0.50$, $\alpha = 55$
t=20s
t=110s
t=200s
t=290s
t=380s
t=470s
h (mm)
x (cm)

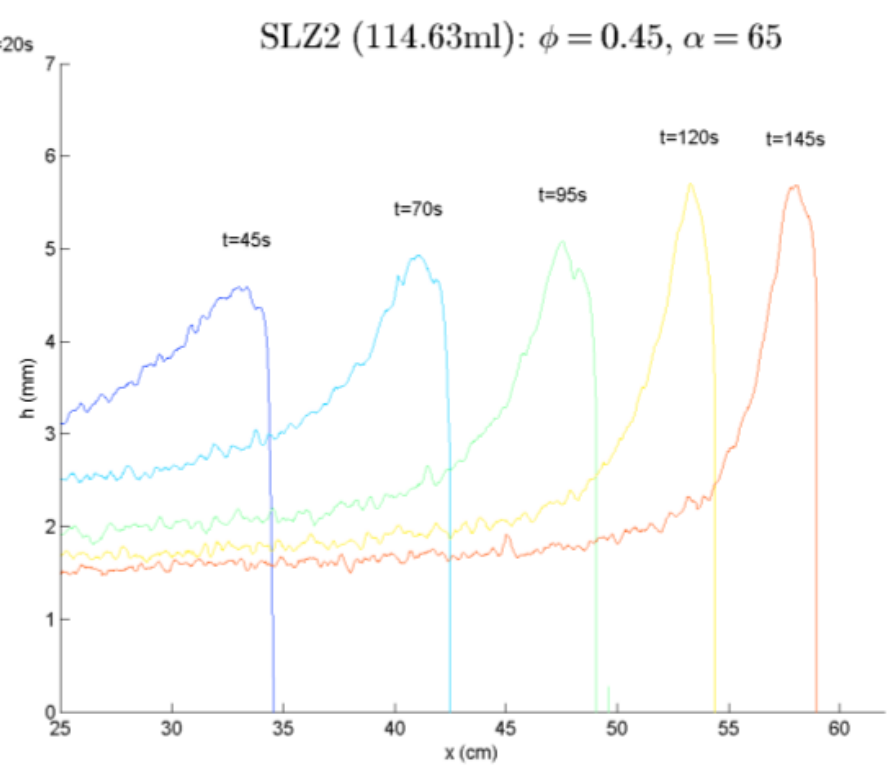
t=20s
SLZ2 (114.63ml): $\phi = 0.45$, $\alpha = 65$
t=45s
t=70s
t=95s
t=120s
t=145s
h (mm)
x (cm)

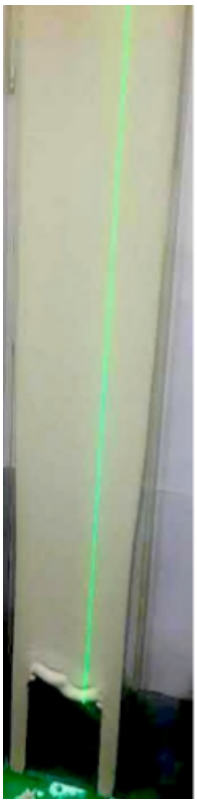

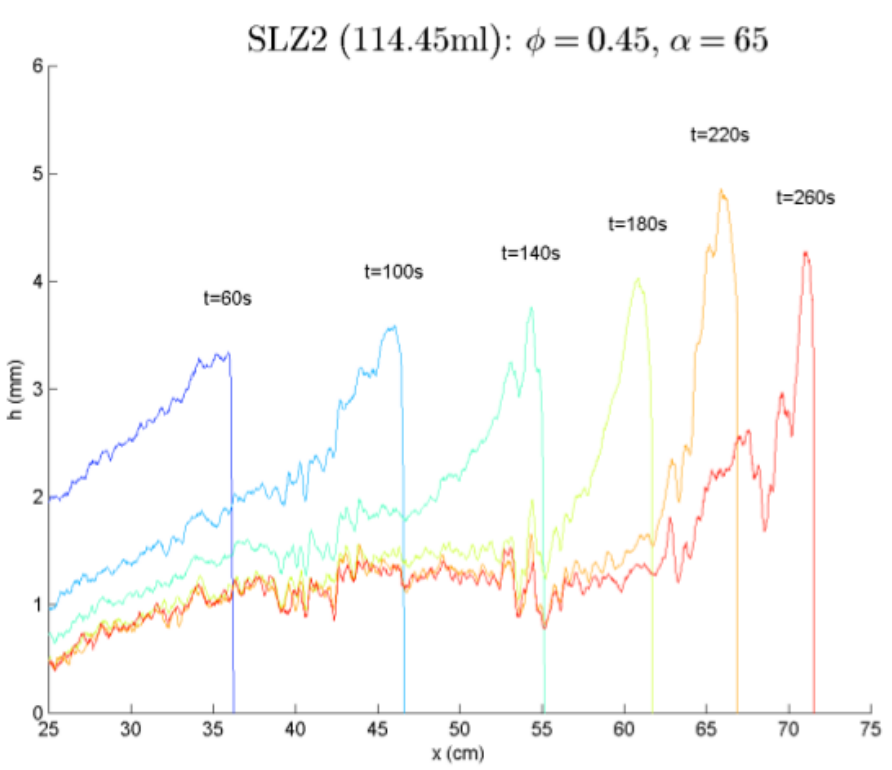
SLZ2 (114.45ml): $\phi = 0.45$, $\alpha = 65$
t=60s
t=100s
t=140s
t=180s
t=220s
t=260s
h (mm)
x (cm)

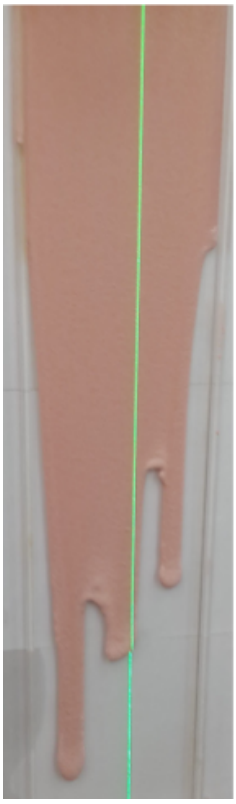

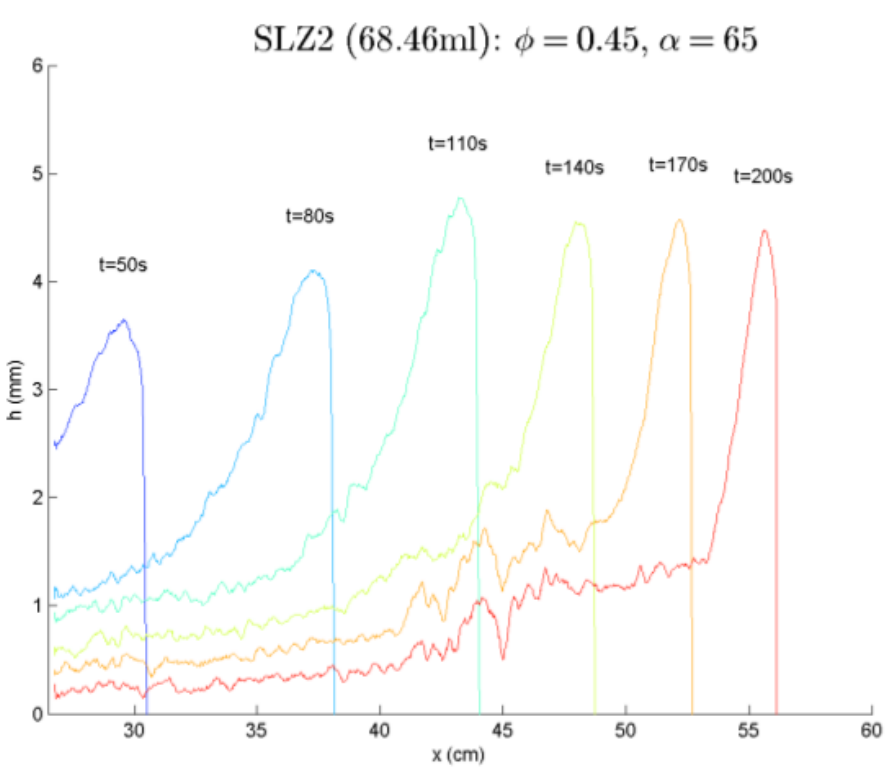
SLZ2 (68.46ml): $\phi = 0.45$, $\alpha = 65$
t=50s
t=80s
t=110s
t=140s
t=170s
t=200s
h (mm)
x (cm)

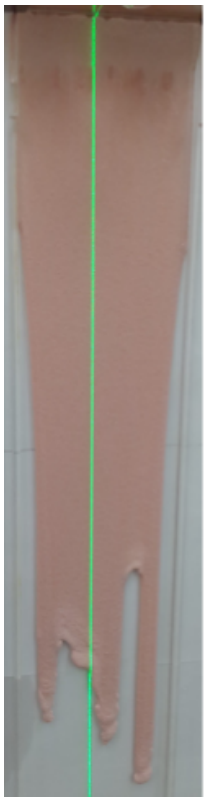

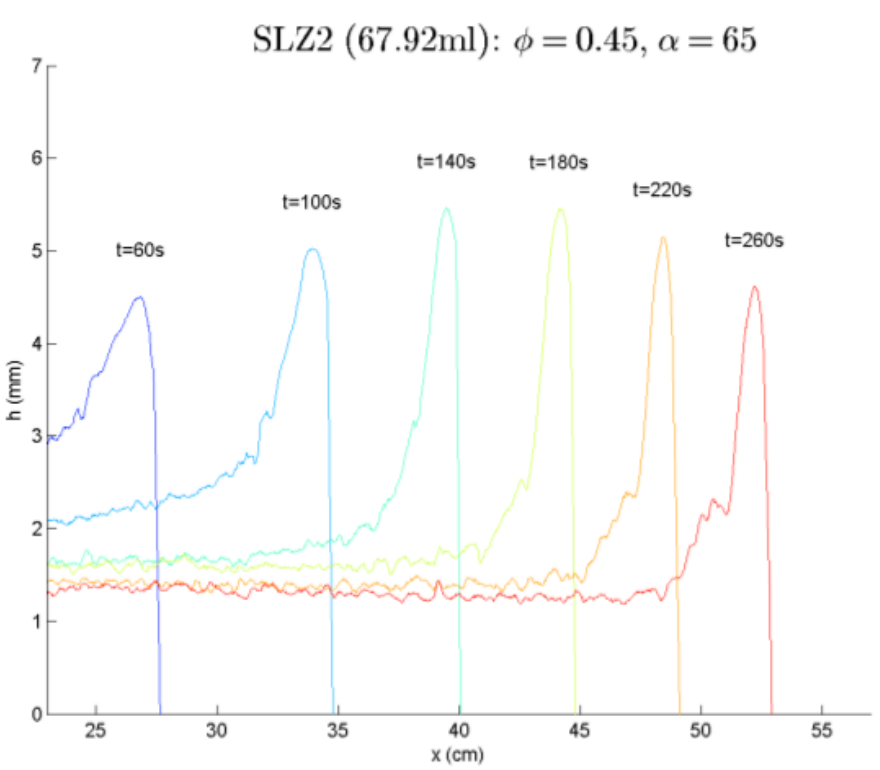
SLZ2 (67.92ml): $\phi = 0.45$, $\alpha = 65$
t=60s
t=100s
t=140s
t=180s
t=220s
t=260s
h (mm)
x (cm)
0
1
2
3
4
5
6
7
25
30
35
40
45
50
55

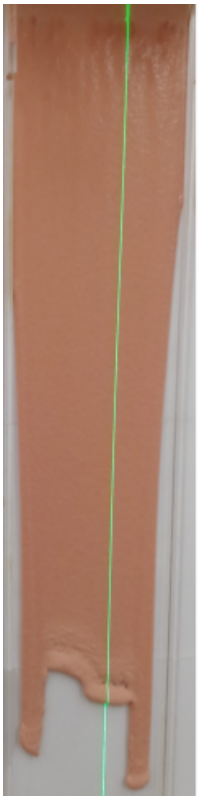

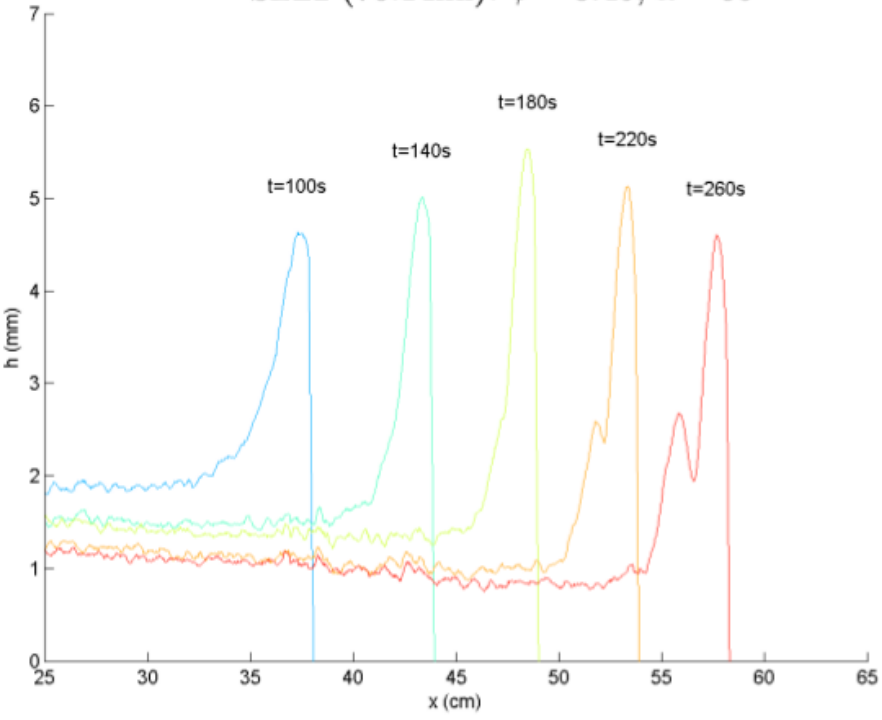
SLZ2 (76.14ml): $\phi = 0.45$, $\alpha = 65$
t=100s
t=140s
t=180s
t=220s
t=260s
h (mm)
x (cm)
0
1
2
3
4
5
6
7
25
30
35
40
45
50
55
60
65

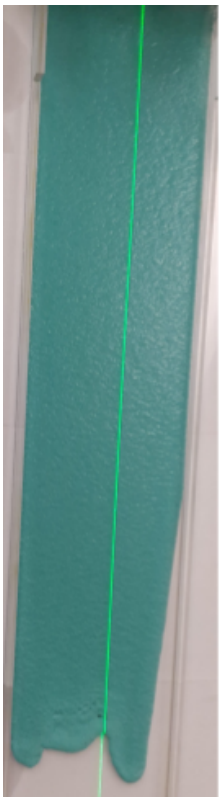

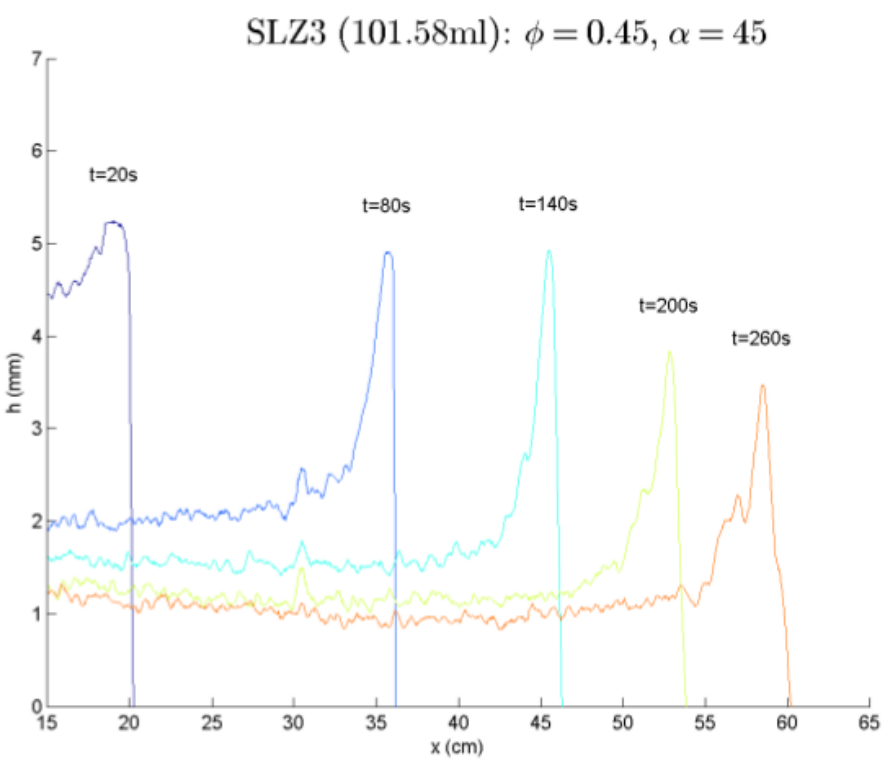
SLZ3 (101.58ml): $\phi = 0.45$, $\alpha = 45$
t=20s
t=80s
t=140s
t=200s
t=260s
h (mm)
x (cm)

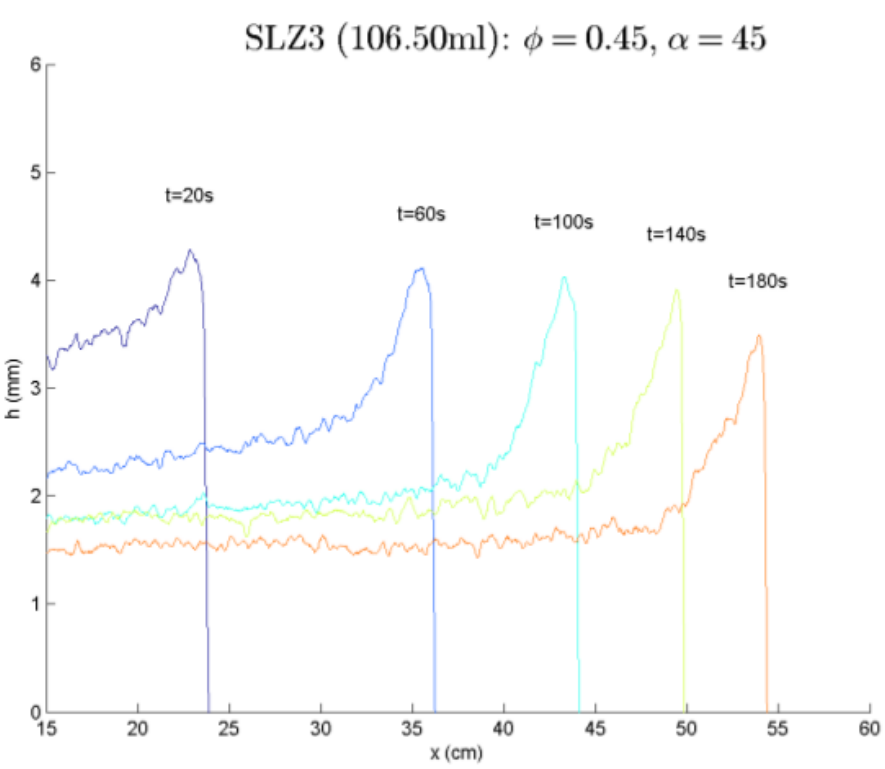
SLZ3 (106.50ml): $\phi = 0.45$, $\alpha = 45$
t=20s
t=60s
t=100s
t=140s
t=180s
h (mm)
x (cm)

4.4.1 Volume Comparison

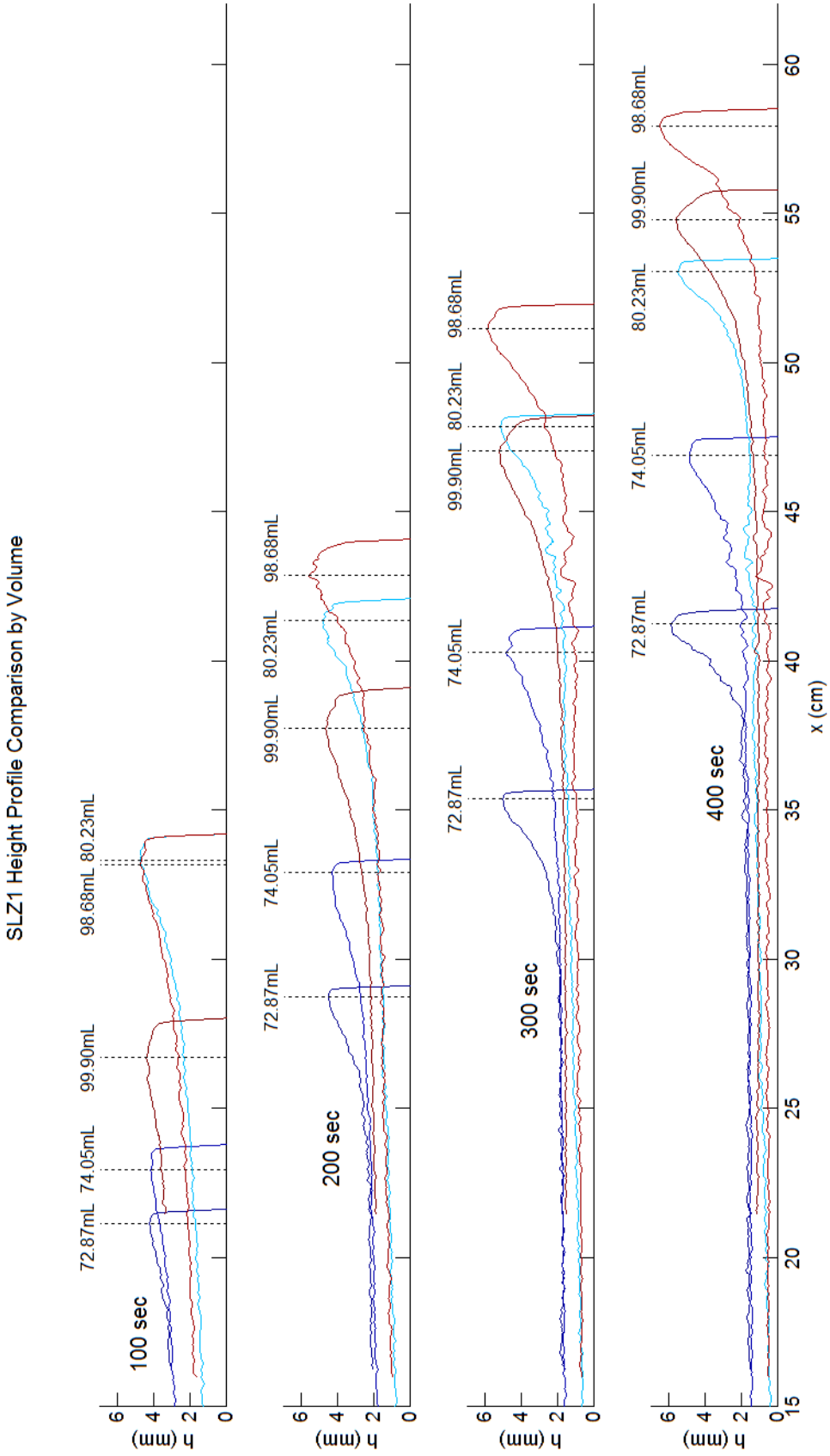

Figure 17: Comparing experiments of the same parameters but different volumes. This is done to vary the relative precursor height.

4.5 Numerical Results

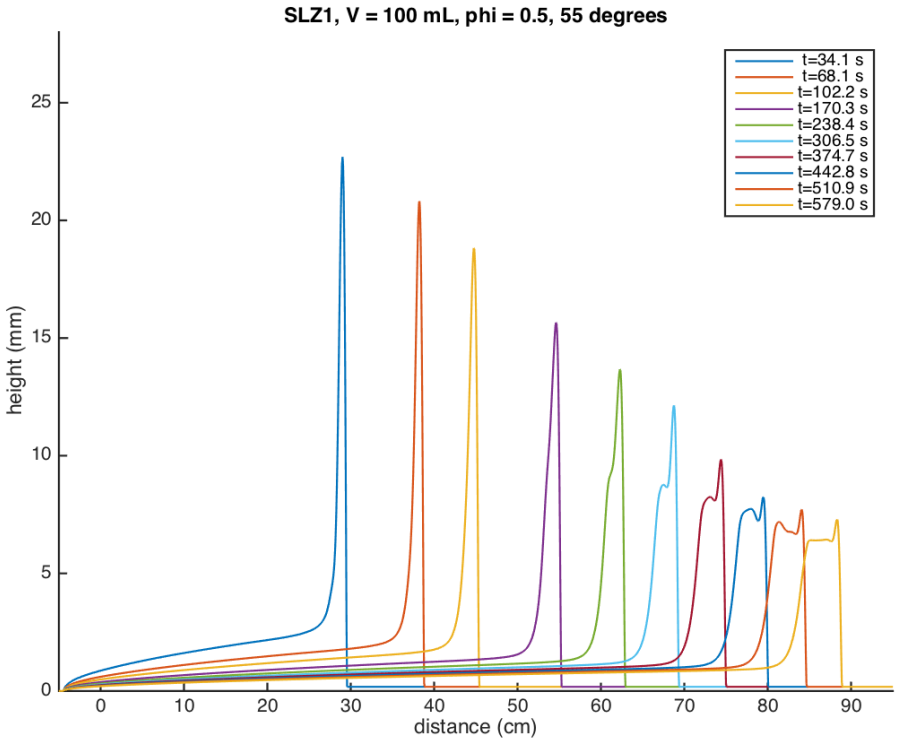

Figure 18: $\beta = 0.01$, $h_{\text{prec}} = 0.01$

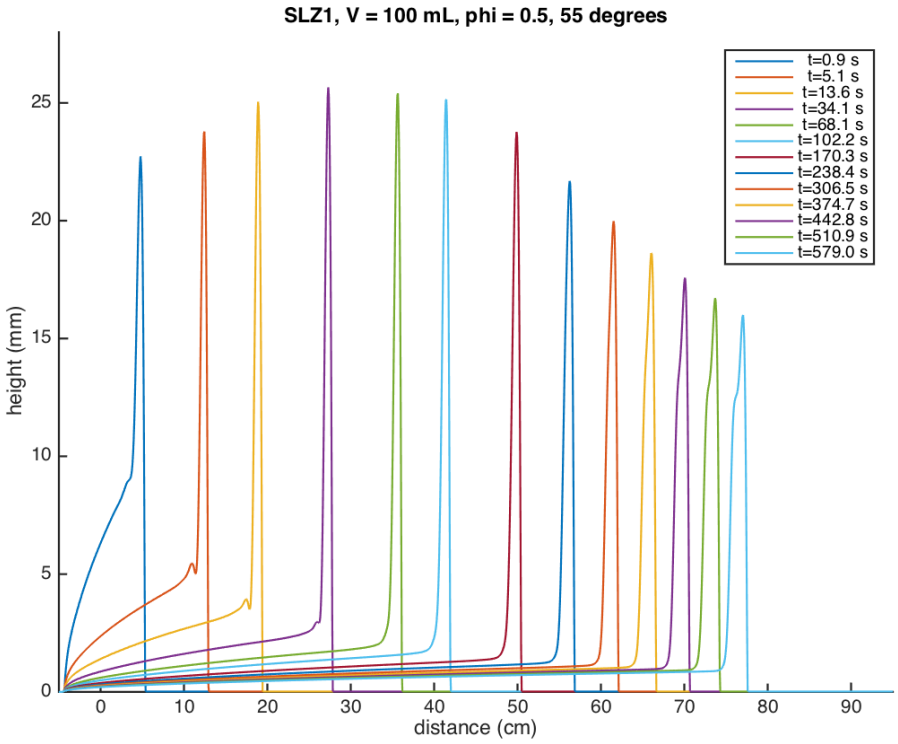

Figure 19: $\beta = 0.01$, $h_{\text{prec}} = 0.001$

One of the goals this summer was to compare the results of our height profile experiments to the corresponding numerical model. However, it can be seen that the numerical models have different attributes than the experimental data presented. For example, the numerical model does not capture the transient period. In the experiments, we see a tall initial condition followed by a relatively flat well-mixed period and then finally the formation of the ridge. For our numerical simulations we attempted to replicate the initial conditions of the experiment, from which we observed a ridge which briefly increases in height and then decreases. Our experimental evidence only shows an increase in height of the ridge over time, however we also acknowledge that our procedure only records height profiles after a certain distance from the gate at $x = 0$ (typically 10 cm to 30 cm). Another thing to note is the height in the numerics is not very physical. In the experiments we observe the maximum height of the ridge to be at about 6 mm but in the numerics the height is around $7-25$ mm.

In the numerical simulations we also compare the effects of the precursor height on the formation of the shock. In the two figures in this section, all parameters are kept the same but the precursor height is reduced by a factor of 10. Reducing the precursor height causes the ridge height to increase and also the shock to move slower in the x-direction.

5 Conclusion and Outlook

5.1 Finger Instability

We were able to conduct numerous experiments in order to better understand the fingering instability, especially as it relates to surface tension. However, given more time, we would like to further analyze why particle diameter was correlated with quantity of fingers. We would like to conduct more experiments in order to better understand the relationship and true dependence of particle size and quantity of fingers. We would also like to understand this dependence in terms of our model, as currently our model does not account for particle size. We would also like to conduct more experiments and vary our procedure for the finger concentration experiments. Our early results were promising as $\phi_{initial} < \phi_{finger} < \phi_{max}$. We were unable to systematically perform experiments varying one parameter at a time and we would still like to play with our procedure in order to optimize its efficiency, accuracy, and reproducibility.

5.2 Height Profile

The intention of measuring the shock front this summer was to be able to compare it closely to the numerical model. Some of the settings in the experiment had not been previously matched in the numerics such as the initial condition and the precursor height. In the numerics, the initial condition does not have much effect on the development of the shock as it progresses, but it is important to us that it be similar to what is seen in the experiment. When the slurry is poured into the gate, situated at a high angle for the ridged regime, the mixture accumulates on the gate and doesn't fill the bottom of the reservoir evenly. This makes it seem like the initial condition should be shaped like a triangle, however, we have to consider what it looks like the moment we remove the gate and start the experiment. This could be imagined as a gaussian blob skewed in the direction of gravity. This gave weird results in the experiment, so instead we use a top hat function that goes about 2/5 into the reservoir and has a height scaled according to the volume. However, since the model doesn't account for the transient, this initial condition looks like it increases in height which is not physically seen in the experiment. Instead, we wondered if the initial condition should be the shape of the slurry at the end of the transient. To do this, we would have to look at experiments and find where the transient stage ends according to the data. Then, an ideal slurry would have to be built so that the actual volume is retained. Finally, we would see the ridge form from the initial condition/transient as it appropriately increases in height.

The most important free parameter that affects the formation of the shock is the precursor height. In our experiments, the procedure for establishing the precursor height is to pour less viscous fluid on the track and then use a squeegee to remove visible abnormalities and establish a smooth pre-layer. This pre-layer is so thin that in our current setup there is no way for it to be measured in the lab. One idea was to predict the height theoretically, but this is difficult and would have a large error. For future work, we would like to develop a way to create a thicker pre-layer of uniform height. In the past this was done by letting the

oil drip down the track overnight, but the uniformity of this pre-layer was questionable.

Acknowledgments

We would like to thank our mentors Jeffrey Wong and Li Wang for their guidance and the particle-laden fluid model. We would also like to thank our principal investigator Professor Andrea Bertozzi, UCLA, and NSF grants DMS-1312543 and DMS-1045536 for providing us with this research opportunity.

References

[1] Sarah Burnett, Andrew Li, Matt Molinare, and Katherine Varela. Particle-laden flows. *UCLA Applied Mathematics REU*, 2014.

[2] L. Wang Mavromoustaki, A. and A.L. Bertozzi. Modeling and simulation of particle-laden flow with surface tension. 2015.

[3] N Murisic, J Ho, V Hu, P Latterman, T Koch, K Lin, M Mata, and AL Bertozzi. Particle-laden viscous thin-film flows on an incline: Experiments compared with a theory based on shear-induced migration and particle settling. *Physica D: Nonlinear phenomena*, 240(20):1661–1673, 2011.

[4] Nebojsa Murisic, Benoit Pausader, Dirk Peschka, and Andrea L Bertozzi. Dynamics of particle settling and resuspension in viscous liquid films. *Journal of Fluid Mechanics*, 717:203–231, 2013.

[5] Li Wang and Andrea L Bertozzi. Shock solutions for high concentration particle-laden thin films. *SIAM Journal on Applied Mathematics*, 74(2):322–344, 2014.

[6] Li Wang, A Mavromoustaki, AL Bertozzi, G Urdaneta, and K Huang. Rarefaction-singular shock dynamics for conserved volume gravity driven particle-laden thin film. *Physics of Fluids (1994-present)*, 27(3):033301, 2015.

A Data for Finger Growth Experiments

All experiments used GSB7 at phi=.45, initial vol=110mL

Angle/Trial	Actual Volume	Theoretical transient length	Observed transient length-ish	Number of fingers at end of transient stage	Number of fingers at end	Average length of fingers at transient stage	Average length of fingers at end	Distance
70/I	95.67mL	56.66cm	35cm	3	3	6.83cm	10.83cm	Broke at 73cm
70/II	96.52mL	53.65cm	35cm	2	1	5cm	11cm	Broke at 75cm
70/III	97.25mL	45.22cm	35cm	2	2	5cm	10cm	Broke at 85cm
67.5/I	102.84mL	70.06cm	35cm	3	3	9cm	12cm	Broke at 70cm
67.5/II	102.59mL	69.69cm	40cm	2	2	7cm	11cm	Ended at 70cm
67.5/III	102.17mL	55.91cm	35cm	3	3	7cm	14cm	Ended at 75cm
65/I	98.41mL	48.13cm	35cm	2	2	5cm	9cm	Broke at 73cm
65/II	103.20mL	55.51cm	35cm	2	2	7cm	10cm	Broke at 73cm
65/III	102.78cm	50.57cm	40cm	3	3	5cm	7cm	Broke at 75cm
62.5/I	103.63mL	38.26cm	35cm	2	2	2cm	6cm	Broke at 80cm
62.5/II	101.99mL	32.65cm	40cm	2	2	7cm	9cm	Broke at 83cm
62.5/III	100.95mL	23.97cm	40cm	4	3	9cm	10cm	Broke at 75cm
60/I*	101.32mL	48.12cm	40cm	0	0	NA	NA	Broke at 70cm
60/II*	100.95mL	59.44cm	40cm	0	0	NA	NA	Broke at 65cm
60/III*	102.59mL	62.40cm	40cm	0	0	NA	NA	Broke at 65cm
60/IV*	102.17mL	61.62cm	35cm	0	0	NA	NA	Broke at 65cm
60/V	98.34mL	35.78cm	35cm	4	3	3cm	2cm	Broke at 75cm
60/VI	100.59mL	34.04cm	40cm	2	2	6cm	7cm	Broke at 78cm
60/VII	101.62mL	39.47cm	40cm	2	2	15cm	17cm	Stopped at 75cm

*The first four trials at 60 degrees used particles that we believe were contaminated. These four trials were not used in calculating final results.

Figure 20: A compilation of all data sampled from finger growth experiments.